FEBS Letters 583 (2009) 983–991

FEBS Letters

journal homepage: www.FEBSLetters.org

Molecular and functional characterization of the plastid-localized Phosphoenolpyruvate enolase (ENO1) from *Arabidopsis thaliana*

Veena Prabhakar, Tanja Löttgert, Tamara Gigolashvili, Kirsten Bell, Ulf-Ingo Flügge, Rainer E. Häusler *

Universität zu Köln, Botanisches Institut, Gyrhofstrasse 15, D-50931 Köln (Cologne), Germany

ARTICLE INFO

Article history:
Received 19 January 2009
Revised 9 February 2009
Accepted 9 February 2009
Available online 15 February 2009

Edited by Julian Schroeder

Keywords:
Plant glycolysis
Plastid enolase
Phosphoenolpyruvate
Enzyme kinetics
Trichomes
Phosphate translocator

ABSTRACT

The *Arabidopsis thaliana* gene At1g74030 codes for a putative plastid phosphoenolpyruvate (PEP) enolase (ENO1). The recombinant ENO1 protein exhibited enolase activity and its kinetic properties were determined. ENO1 is localized to plastids and expressed in most heterotrophic tissues including trichomes and non-root-hair cells, but not in the mesophyll of leaves. Two T-DNA insertion *eno1* mutants exhibited distorted trichomes and reduced numbers of root hairs as the only visible phenotype. The essential role of ENO1 in PEP provision for anabolic processes within plastids, such as the shikimate pathway, is discussed with respect to plastid transporters, such as the PEP/phosphate translocator.

1. Introduction

Phosphoenolpyruvate is a central intermediate of metabolism in pro- and eukaryotes. The glycolytic sequence starting from 3-phosphoglycerate (3-PGA), involving phosphoglyceromutase (PGyM) and enolase (ENO), appears to be the main route for the production of phosphoenolpyruvate (PEP), e.g. [1]. Besides glycolysis [2,3], in plants, PEP can also be formed from pyruvate by PPDK (pyruvate, orthophosphate dikinase, which is an essential step in C_4- and crassulacean acid metabolism (CAM)-plants [4], but occurs also in C_3-plants [5–7], or from oxaloacetate in gluconeogenesis [8] by PEP carboxykinase (PEPCK) [9,10]. Whereas PPDK in *Arabidopsis thaliana* has been shown to be dually targeted to the cytosol and the plastids [7], PEPCK is localized to the cytosol of plants [9,10]. In the catabolic direction, PEP is further metabolized to pyruvate by the action of pyruvate kinase (PK), yielding pyruvate, which can enter the citric acid cycle to generater NADH and ATP by the respiratory chain in the mitochondria [11]. Besides their catabolic function for energy generation in heterotrophic tissues or in leaves during the dark period, both PEP and pyruvate represent essential precursors for anabolic reactions. PEP, together with erythrose 4-phosphate, is fed into the shikimate pathway, which is localized within the plastid stroma [12–14]. The shikimate pathway is essential for the production of aromatic amino acids and a huge variety of secondary plant products. In turn, pyruvate can act as a precursor (i) for fatty acid biosynthesis [15,16], (ii) for the synthesis of branched-chain amino acids [17], and together with glycerinaldehyde 3-phosphate (iii) for the mevalonate-independent way (2-C-methyl-D-erythritol 4-phosphate [MEP] pathway) of isoprenoid biosynthesis [18]. All these pathways are entirely localized to the plastid stroma. Moreover, PEP can be imported into the plastids *via* the PEP/phosphate translocator (PPT) for e.g. the production of aromatic amino acids [19–22]. The genome of *A. thaliana* contains two *PPT* genes (*AtPPT1* and *AtPPT2*), which are differentially expressed and are found both in photoautotrophic and heterotrophic tissues [20]. The reticulate leaf phenotype of the

Abbreviations: BCIP, 5-bromo-4-chloro-3′-indolyl phosphate; BSA, bovine serum albumin; CAM, crassulacean acid metabolism; CaMV, cauliflower mosaic virus; CDS, coding sequence; *cue*, *chlorophyll a/b binding protein underexpressed*; DPGA, diphosphoglyceric acid; ENO, enolase; GAPDH, glyceraldehyde 3-phosphate dehydrogenase; GFP, green fluorescent protein; Glc6P, glucose 6-phosphate; GPT, glucose 6-phosphate/phosphate translocator; GUS, β-glucouronidase; IgG, immunoglubulin G; IPTG, isopropyl-β-D-thiogalactopyranoside; LDH, lactate dehydrogenase; MEP, 2-C-methyl-D-erythritol 4-phosphate; NBT, nitroblue tetrazolium chloride; Ni–NTA, Ni–nitrilotriacetic acid; OPPP, oxidative pentose phosphate pathway; PCR, polymerase chain reaction; PEP, phosphoenolpyruvate; PEPCK, phosphoenolpyruvate carboxykinase; PFD, photon flux density; PGA, phosphoglyceric acid; PGK, phosphoglycerate kinase; PGyM, phosphoglycerate mutase; PK, pyruvate kinase; PPDK, pyruvate, orthophosphate dikinase; PPT, phosphoenolpyruvate/phosphate translocator; RT-PCR, Reverse transcriptase polymerase chain reaction; SDS–PAGE, sodium dodecyl sulfate polyacrylamide gel electrophoresis; TPT, triose phosphate/phosphate translocator; UTR, untranslated region

* Corresponding author. Fax: +49 221 470 5039.
E-mail address: rainer.haeusler@uni-koeln.de (R.E. Häusler).

0014-5793/$36.00
doi:10.1016/j.febslet.2009.02.017

chlorophyll a/b binding protein underexpressed1 (*cue1*) mutant [23] defective in AtPPT1 could be rescued by feeding a cocktail of aromatic amino acids to the mutants [21]. The ectopic expression of a C_4-type plastid-localized PPDK also rescued the *cue1* phenotype, in that PEP could be produced from pyruvate within those plastids, where AtPPT1 was missing [22]. Although there is biochemical evidence that pyruvate can also be imported across the plastid envelope [24,25], a specific pyruvate transport protein remains to be identified. It appears therefore also likely that stromal pyruvate derives predominantly from PEP *via* the reaction catalyzed by PK, which in addition to pyruvate delivers one molecule of ATP for each PEP consumed. The obvious way to provide PEP, i.e. *via* glycolysis, appears not to operate in most plastids. Chloroplasts and some non-green plastids (i.e. from cauliflower buds) appear to lack either PGyM or ENO or both [17,26–30], whereas plastids from lipid storing seeds, i.e. canola or castor bean, have been shown to contain a complete set of glycolytic enzymes [31–34].

The genome of *A. thaliana* contains three putative *ENO*- and 15 putative *PGyM* genes (e.g. TAIR; http://www.arabidopsis.org/). Of the *PGyM* genes, four genes code for proteins with predicted N-terminal transit peptides for plastid targeting. In contrast, there is only one putative ENO (ENO1), which is highly likely to be localized in the plastids (http://aramemnon.botanik.uni-koeln.de/). Moreover, *in silico* expression analyzes based on microarray data (http://bar.utoronto.ca/efp/cgi-bin/efpWeb.cgi) revealed high expression levels of *ENO1* in roots and siliques (i.e. during embryo development), but a low expression in green tissues, such as leaves or stems. In constrast, three of the four putative plastidic PGyM genes are also highly expressed in photosynthetic tissues, suggesting that glycolysis in chloroplasts might proceed to 2-PGA, but not further to PEP and pyruvate. To elucidate the role of plastid glycolysis in PEP provision for biosynthetic reactions, the putative plastid *ENO1* gene was cloned and the ENO1 protein containing a C-terminal hexa-histidine-tag heterologously expressed in *Escherichia coli.* Using specific enzyme assays, the catalytic function of ENO1 could be verified and relevant kinetic constants determined. The tissue- and cell-specific expression profile of *ENO1* and the lack of a severe phenotype of *eno1* knock-out mutants are discussed with respect to the role of both AtPPTs, which mediate a PEP/Pi- or PEP/2-PGA counter exchange across the plastid envelope.

2. Materials and methods

2.1. Plant material and growth

Wild-type and mutant *A. thaliana* plants, ecotype Colombia were used in all experiments. The *eno1* mutant alleles (*eno1-1*; N616157 and *eno1-2*; N421734) were provided by the Nottingham Arabidopsis Stock Center (NASC; http://arabidopsis.info/). *Arabidopsis* plants were initially germinated and grown on soil for 4–5 weeks in a temperature-controlled greenhouse at a 17-h-light/7-h-dark-cycle. The average photon flux density (PFD) on plant level was 70–100 μmol m^{-2} s^{-1}. For growth of plants in sterile culture, seeds were surface-sterilized and germinated on agar supplemented with half-strength Murashige and Skoog (MS) medium containing 2% sucrose (Duchefa, Haarlem, Netherlands). Plantlets were grown in a Percival growth cabinet at day/night temperatures of 21 °C/18 °C and a 17-h-light/7-h-dark-cycle at an average PFD of 50–80 μmol m^{-2} s^{-1}.

2.2. Subcellular localization of ENO-GFP constructs in heterotrophic A. thaliana cell cultures

For the subcellular localization of ENO1 (At1g74030) and ENOc (cytosolic ENO, At2g29560) proteins, N-terminal amino acid fragments were translationally fused to green fluorescent protein (GFP). The coding regions of ENO1 and ENOc equivalent to 107 and 101 amino acids, respectively, were amplified by reverse transcriptase polymerase chain reaction (RT-PCR) using the primer pairs *ENO1-GFP sense,* 5′ TC ATGGCTTTGACTACAAAACCTCACCATCTT 3′, *ENO1-GFP antisense,* 5′ CACCTTTACCACCATAGACGCTCT 3′, *ENOc-GFP sense,* 5′ TC ATGTCTGTGCAAGAGTATTTAGACAAGCA 3′, and *ENOc-GFP antisense,* 5′ CAAGATACATTCCTTTGTCTCCATCA 3′, and subjected to Gateway cloning (Invitrogen GmbH, Karlsruhe, Germany). The fragments were cloned into the pDONOR207 vector followed by recombination usind the LR reaction with the pGWB5 destination vector containing a cauliflower mosaic virus (CaMV) 35S driven full-length PAN w/C-terminal GFP. For transient expression of the *ENO1-GFP* and *ENOc-GFP* constructs, an *A. thaliana* suspension cell culture line was generated from roots and maintained in AT-medium according to [35]. One-week-old, dark-grown cultured *A. thaliana* cells were transformed using the super-virulent *Agrobacterium* strain LBA4404.pBBR1MCS.virGN54D (kindly provided by Dr. Memelink, University of Leiden) as described by [36]. GFP fluorescence was visualized with a fluorescence microscope (Leica DM RA2 filter F46-002 ET-Bandpass 470/40).

2.3. Expression of functional ENO1 in E. coli cells and purification by Ni–NTA chromatography

PCR primers were designed for the full length coding sequence (CDS) of ENO1 from *A. thaliana* (At1g74030). A sense primer ENO1-GW-F (5′ CACC**ATG**GCTTTGACTACAAAACC 3′) containing the start codon and an antisense primer lacking the stop codon ENO1-GW-R (5′ TGGTGATCGGAAAGCTTCACCG 3′) was designed for cloning into the Gateway entry vector pENTR SD/D-TOPO harboring a Shine-Dalgarno (SD) sequence for efficient sequence initiation of C-terminal fusion in *E. coli*. The PCRs were run at 95 °C for 2 min followed by 35 cycles (30 s at 95 °C, 30 s at 59 °C and 1 min at 72 °C) and a final extension at 72 °C for 7 min. Full length ENO1 was recombined by LR reaction into the Gateway destination vector pET-DEST42 (Invitrogen GmbH, Karlsruhe, Germany), containing a C-terminal polyhistidine tag (His-tag) and transformed into competent *E. coli* cells (strain BL21; Invitrogen GmbH, Karlsruhe, Germany). *E. coli* cells were grown at 37 °C in 100 ml LB-medium containing 50 μg ml^{-1} carbenicillin, and ENO1 expression was induced by the addition of 1 mM IPTG (isopropyl-β-D-thiogalactopyranoside). The cells were pelleted by centrifugation (4000×*g* for 15 min), resuspended in 100 mM Tris–HCl (pH7.5), 1.5 M NaCl, 2 mM EDTA supplemented with 20 μl ml^{-1} Protease Inhibitor Cocktail (Sigma, P2714) and lysed by sonication (20 cycles, duty cycle 50%, output control 4) with a Branson sonifier 450. The lysate was centrifuged at 4000×*g* for 15 min and the supernatant subjected to Ni–nitrilotriacetic acid (Ni–NTA) affinity chromatography. The supernatant was mixed with 0.5 ml of Ni–NTA agarose (Qiagen, Hilden, Germany) pre-equilibrated with 50 mM NaCl and 100 mM Na-Pi (pH 7.8). The recombinant protein was allowed to bind to the Ni–NTA agarose for 1 h at 4 °C, and after transfer to a column (i.e. a glasswool plugged pasteur pipette), the resin was washed twice with 800 μl of 100 mM Na-Pi (pH 7.8), 8 mM imidazole and ENO1 was specifically eluted in four steps with 100 μl each of 100 mM Na-Pi (pH 7.8) and 150 mM imidazole. ENO1 activity was enriched in the third fraction.

Cell lysates and purified ENO1 preparations were separated by sodium dodecyl sulfate polyacrylamide gel electrophoresis (SDS–PAGE) on 12% separation gels according to Ref. [37] and protein stained with Coomassie Brilliant Blue R-250 (Serva, Heidelberg, Germany). Western blots were performed according to [38] using a Semidry Western transfer apparatus (Itf-Labortechnik GmbH & Co., KG Wasserburg/Bodensee, Germany). The blots were incubated with the primary penta-His-antibody (Qiagen, Hilden,

Germany) followed by the secondary goat anti-mouse immunoglubulin G (IgG) antibody conjugated with alkaline peroxidase and developed in a solution containing 30 mg ml^{-1} NBT (nitroblue tetrazolium chloride), 15 mg ml^{-1} BCIP (5-bromo-4-chloro-3′-indolyl phosphate), 100 mM Tris–HCl (pH 9.5), 100 mM NaCl and 5 mM $MgCl_2$.

2.4. Enolase activity assay and protein determination

Enolase activity was determined spectrophotometrically in coupled enzyme assays according to [31] at 340 nm and a temperature of 25 °C in a microtiter plate reader (Spectrafluor Plus, Tecan, Austria). For the forward (glycolytic) reaction the assay mixture contained in 200 µl, 100 mM Tricine–NaOH (pH 8.0) or 100 mM HEPES–NaOH (pH 7.0), 1 mM $MgSO_4$, 10 mM KCl, 5 mM 3-phosphoglyceric acid (3-PGA), 0.1 mM 2,3-diphosphoglyceric acid (2,3-DPGA), 1 mM ADP, 0.2 mM NADH, 3 U phosphoglycerate mutase (PgyM) from rabbit muscle (Boehringer, Mannheim, Germany), 2 U pyruvate kinase (PK) (Sigma–Aldrich, Steinheim, Germany) and 2.75 U lactate dehydrogenase (LDH) (Roche Diagnostics, Mannheim, Germany). Despite the lack of availability of 2-PGA by chemical supply companies, a residual batch of 2-PGA (Sigma–Aldrich, Steinheim, Germany) was used as the direct substrate at concentrations of up to 5 mM. In the case when 2-PGA was used 2,3-DPGA and PGyM were omitted. For the reverse (gluconeogenic) reaction the standard assay mixture contained 100 mM Tricine–NaOH (pH 8.0) or 100 mM HEPES–NaOH (pH 7.0), 1 mM $MgSO_4$, 10 mM KCl, 5 mM PEP, 0.1 mM 2,3-DPGA, 2 mM ATP, 0.2 mM NADH, 3 U PGyM, 6 U 3-phosphoglycerate kinase (PGK) from baker's yeast (Sigma–Aldrich, Steinheim, Germany) and 3 U glyceraldehyde 3-phosphate dehydrogenase (GAPDH) from rabbit muscle (Roche Diagnostics, Mannheim, Germany). Kinetic constants (K_m, V_{max}) were obtained from hyperbolic curve fits to the experimental data implemented in SigmaPlot8.0 for windows (SPSS Inc.). Protein was determined according to [39] with bovine serum albumin (BSA) as a standard.

2.5. Semiquantitative RT-PCR

Total RNA was extracted from flowers of wild-type *A. thaliana* (ecotype Columbia) using the RNase ALL method [40]. The RNA was treated with DNase I to digest traces of DNA using a DNA-free kit (Ambion, Darmstadt, Germany). The first strand cDNA was synthesized using the BioScript enzyme from Bioline (Luckenwalde, Germany) and its integrity was checked using actin primers *ActinF-Lg* 5′ TAACTCTCCCGCTATGTATGT 3′ and *ActinR-Lg* 5′ CCACTGAGCACAATGTTACCGTAC 3′. For the amplification of the full length CDS of *ENO1* the sense primer *ENO1-GW-F* (5′ CACCATGGCTTTGACTACAAAACC 3′) and the antisense primer *ENO1-GWstop-R* (5′ TCATGGTGATCGGAAAGCTTCACC 3′) were used. The PCRs were run at 95 °C for 2 min followed by 30 cycles (30 s at 95 °C, 30 s at 59 °C and 1 min at 72 °C) and a final extension at 72 °C for 7 min. The PCR products were separated on 1% agarose gels.

2.6. Construction of β-glucouronidase (GUS) reporter vectors and plant transformation

ENO1 promoter-GUS constructs were generated as translational fusions of DNA fragments comprising three individual promoter and/or putative regulatory regions designated as A, AB, and C) to the *uidA* gene. The individual *ENO1 promoter* constructs consisted of a 306 bp fragment upstream of the translational start including the complete intergenic region in front of At1g74040 and the 5′-untranslated region (5′-UTR) (A), a fusion of construct A with a 676 bp fragment downstream of the translational stop including the 3′-UTR (AB) [41,42], and (C) a 1312 bp fragment including fragment A, the first exon, the first intron and parts of the second exon.

To generate construct A, 306 bp of the sequences at the 5′-UTR region before the ATG of *ENO1* were amplified with the primers *ENO1(A)* sense 5′ ACGGCACAGTGTCTCTGGTTACTACTTTGCTAGTG and *ENO1(A)* antisense CCTCTTCGATACGGCAAAGCCATTACACGATACCT. For the generation of construct AB, initially 676 bp of B (i.e. the 3′-UTR region of *ENO1*) was amplified using the primers *ENO1(B)* sense 5′ CACCGTAATGGCTTTGCCGTATCGAAGAGGAACTCG and *ENO1(B) anti*sense 5′ GAACTTGCTCACAGCTCCACATAATTTCCTTCA 3′ and fused to construct A by PCR yielding a product of 982 bp. To generate construct C, which included the sequence of construct A, primers *ENO1(A)* sense 5′ ACGGCACAGTGTCTCTGGTTACTACTTTGCTAGTG 3′ and *ENO1(C) anti*sense 5′ CATAAACTCTTGCATAGCCAAACTATTCCCAGCATG 3′ were used to amplify a product of 1312 bp. The PCR products (A, AB and C) were cloned into the Gateway entry vector pENTR D-TOPO and recombined using *attB* recombination (Invitrogen GmbH, Karlsruhe, Germany) into the pGWB3 destination vector. The constructs were transformed into *Arabidopsis* wild-type plants and 20 transgenic lines containing the individual constructs selected by kanamycin were analyzed for GUS expression. GUS staining was performed according to [43] overnight at 37 °C.

3. Results

3.1. Identification, subcellular localization and purification of the A. thaliana ENO1

The *A. thaliana* genome contains three genes annotated as putative *ENOs* (At2g29560, At2g36530, At1g74030). According to the *Aramemnon* database [44], At1g74030 encodes a protein

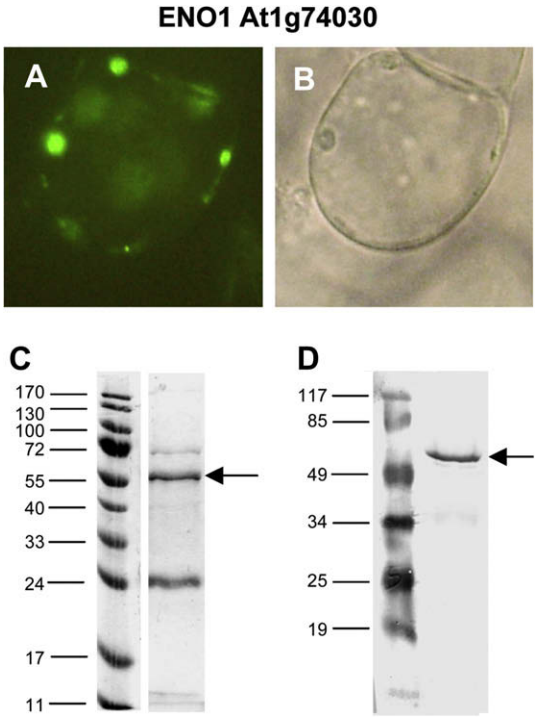

Fig. 1. Subcellular localization of ENO1 and purification of recombinant ENO1 protein. The ENO1-GFP fusion protein was transiently expressed in a heterotrophic *A. thaliana* cell culture. A Transformed cell is shown as a microscopic fluorescence image (exc, 485 nm; em, 530 nm) (A) compared to a bright field image (B) of the same cell. (C) Separation of a Ni-NTA purified ENO1 preparation by SDS–PAGE and detection of the recombinant protein by Western blot analysis using an anti-hexahistidine-tag antibody (D).

containing an N-terminal transit peptide for plastid targeting with a consensus prediction (i.e. its probability) of 15.8 compared to 0.6 and 0.0 for At2g36530 and At2g29560, respectively (http://aramemnon.botanik.uni-koeln.de/). For one of the two putative cytosolic ENO proteins (At2g36530, equivalent to AtLOS2), a dual targeting has been shown recently [45]. A LOS2-GFP fusion protein was located both in the cytosol and in the nucleus. The subcellular localization of the putative plastidic ENO (i.e. ENO1) and the second cytosolic ENO (ENOc; At2g29560) was investigated after fusion of protein fragments to GFP and transient expression in a heterotrophic *A. thaliana* cell culture. The ENO1-GFP fusion protein (Fig. 1A) was localized within the plastids (Fig. 1B). As a positive control for plastid targeting, GFP was fused to a fragment of the triose phosphate/phosphate translocator (TPT; At5g46110) and expressed in the same *A. thaliana* cell culture (data not shown). In contrast, the GFP-ENOc fusion protein was found both in the cytosol (Supplementary Fig. 1A and B) and the nucleus (Supplementary Fig. 1C and D) and its subcellular localization hence resembles that of AtLOS2. In order to functionally characterize ENO1, the cDNA was fused to a C-terminal His-tag, the construct expressed in *E. coli* and the ENO1 protein enriched by Ni-NTA chromatography. Separation of the final preparation by SDS–PAGE revealed three major protein bands (Fig. 1C) with apparent molecular masses (M_r) of 77.0 kDa, 61.2 kDa and 23.7 kDa. On Western blots only one band (Fig. 1D) corresponding to a M_r of 60.3 kDa emerged using an anti-His antibody. This band was identical to the protein band after SDS–PAGE with an apparent M_r of 61.2 kDa. Based on the amino acid sequence of the ENO1 protein, a M_r of 51.5 kDa can be calculated, which is lower compared to the apparent M_r. As estimated densitometerically after SDS–PAGE, approximately 49% of the total protein consisted of ENO1 (data not shown).

3.2. Kinetic characterization of ENO1 activity

The enriched recombinant ENO1 preparation after Ni–NTA chromatography was analyzed for ENO activity using a standard assay (i.e. in the direction of PEP formation at pH 8.0) with either 3-PGA or 2-PGA as substrates. The specific activity of ENO was between 0.25 and 0.30 U mg^{-1} protein. Considering that about half of the protein on the gel was in the ENO1 protein band identified after SDS–PAGE and on Western blots, the maximum specific activity was calculated to be in the range between 0.5 to 0.6 U mg^{-1} protein. As a control, lysates of wild-type or transformed *E. coli* cells, before induction of ENO1 expression by IPTG, were subjected to Ni–NTA chromatography. No ENO activity could be detected in either case (data not shown). Moreover, ENO activity in crude cell lysates was increased 8-fold and 11-fold upon induction with IPTG compared to lysates prepared from un-induced and wild-type *E. coli* cells, respectively. The specific ENO activity was further increased by a factor of 14 after Ni–NTA chromatography (data not shown). For a further kinetic characterization, the relative reaction velocity (v) observed for saturating 2-PGA concentrations at pH 8.0 was referred to the highest ENO1 activity (100%). The pH response curves shown in Fig. 2 revealed distinct pH optima for the forward (PEP formation) and reverse (2-PGA formation) reaction. For the forward direction, there was a sharp pH-optimum between pH 7.5 and pH 8.5 compared to the reverse reaction, which exhibited a broader pH-optimum between pH 6.0 and pH 7.5. Substrate dependencies of ENO1 activity in the forward and reverse reaction obeyed Michaelis-Menten kinetics (Supplementary Fig. 2A–D), with apparent K_m values for the respective substrates in the submillimolar range (Table 1). At pH 8.0 the V_{max} of the forward direction was more than doubled compared to the V_{max} of the reverse reaction (Table 1, Fig. 2). In particular, the affinity for 2-PGA was high at pH 8, with a K_m in the upper micromolar range (Table 1). In general, the K_m values for both substrates were higher at pH 7.0 as compared to pH 8.0 (Table 1). The kinetic constants determined at pH 7.0 and pH 8.0 were used to calculate the equilibrium constants for the ENO reaction at both pH values by applying the Haldane equation, e.g. [46],

$$K_{eq} = \frac{V_{max(2-PGA)} \cdot K_{m(PEP)}}{V_{max(PEP)} \cdot K_{m(2-PGA)}}, \quad \text{(see Table 1)},$$

The thermodynamic equilibrium favors the formation of PEP from 2-PGA, with K_{eq}-values of 5.66 and 3.45 at pH 8.0 and pH 7.0, respectively (Table 1) and is hence close to the reported value of 6.7 [47]. Moreover, from the ratios of the apparent K_m values for 3-PGA and 2-PGA, the thermodynamic equilibrium for the PGyM reaction could be estimated at both pH values (Table 1).

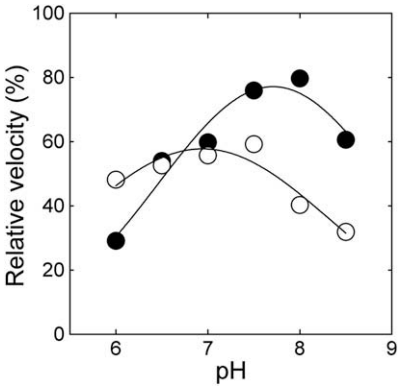

Fig. 2. pH dependency of the ENO1 reaction velocity. ENO1 activity was determined at saturating substrate concentrations either in the direction of PEP- (●) or 2-PGA formation (○). The data are the mean of two independent measurements. The standard deviation was below 5% of the mean (not shown).

Table 1
Kinetic constants of recombinant ENO1 in the forward (2-PGA consumption) and reverse reaction (PEP consumption).

Substrate	pH 8.0			pH 7.0		
	K_m (mM)	V_{max} (%)	K_{eq}	K_m (mM)	V_{max} (%)	K_{eq}
2-PGA	0.082 ± 0.011	100.0 ± 2.7	5.66	0.149 ± 0.008	59.4 ± 0.8	3.45
PEP	0.180 ± 0.058	38.8 ± 2.1		0.534 ± 0.166	61.6 ± 5.6	
3-PGA	1.281 ± 0.097	100.0 ± 2.8	15.62*	0.390 ± 0.095	59.3 ± 3.3	2.62*

The equilibrium constants (K_{eq}) were calculated according to the Haldane equation, whereas the K_{eq} for the PgyM reaction* was estimated from the K_m (3-PGA)/K_m (2-PGA) ratios at both pH values.

3.3. Tissue- and cell-specific expression profiles of AtENO1

The temporal and spatial expression profile of ENO1 was investigated both by semi-quantitative RT-PCR and *promoter::reporter* gene fusions (Fig. 3). The mRNA abundance of *ENO1* was high in young roots and young siliques as well as in the shoot apex, but low in young leaves, stems and cotyledons. It was virtually absent from mature leaves and flowers (Fig. 3A). In order to study the expression of *ENO1* at the cellular level, transgenic *A. thaliana* plants were generated carrying three different *ENO1 promoter::GUS* gene fusion constructs (Supplementary Fig. 3A). For the promoter construct A, there was no GUS staining detectable, indicating that relevant regulatory *cis*-acting elements were missing in this fragment (data not shown). As shown in Fig. 3C–H, the tissue-specific expression profile with the promotor-fusion-construct AB (Fig. 3B) matched very well with RT-PCR data (Fig. 3A) and *in silico* expression profiles based on microarray data (i.e. http://bar.utoronto.ca/

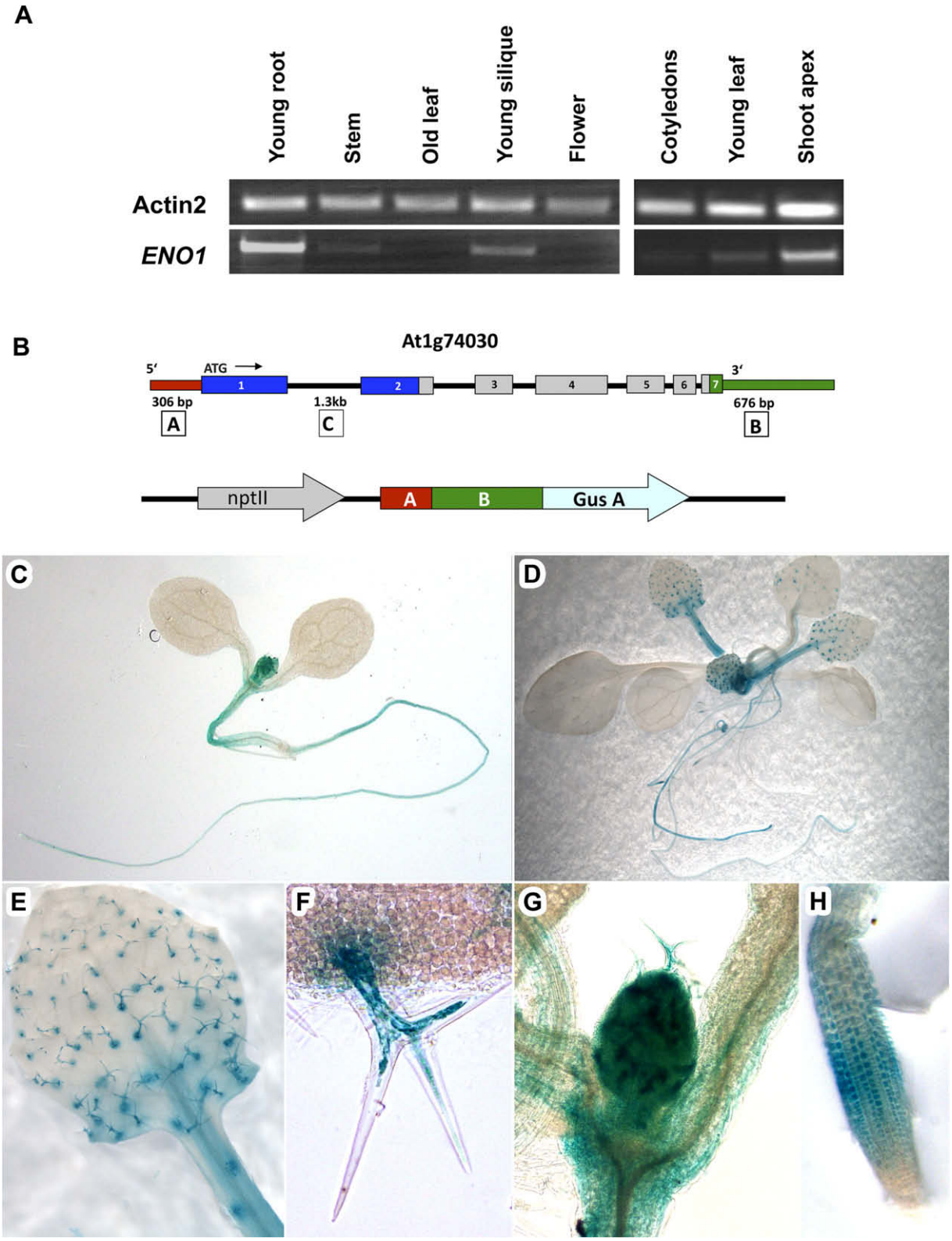

Fig. 3. Analyzes of ENO1 expression by RT-PCR (A) or in transgenic plants (C–H) expressing an *ENO1 promoter::GUS* construct (B). *ENO1* promoter activity indicated by GUS staining of a seedling (C), a mature plant (D) trichomes on a young leaf (E), a mature trichome (F), the shoot apex (G) and the root elongation zone (H).

efp/cgi-bin/efpWeb.cgi). In particular, mature leaves were free of GUS activity (Fig. 3D), and in roots expression was found only in an early developmental state (Fig. 3D). Moreover, the shoot apex (Fig. 3C and G) and the hypocotyls (Fig. 3C) exhibited substantial GUS activity. Similar to the RT-PCR data, cotyledons were devoid of GUS activity (Fig. 3A and C). Apart from the spatial and temporal expression profiles of different organs, interesting insights in *ENO1* expression emerged at the cellular level. *ENO1* expression in roots is restricted to the cortex (in particular to the non-root-hair cells of the rhizodermis) and the central cylinder of the elongation zone

(Fig. 3H). There was no expression at the root tip or basal parts of the roots. High GUS activity was found in trichomes of emerging leaves (Fig. 3D–F), whereas trichomes of mature leaves were devoid of GUS activity (Fig. 3D). Moreover, GUS activity was also high in the meristematic regions of emerging leaves and the petioles (Fig. 3D and F). With the promotor construct C a similar, but not identical, spatial and temporal expression profile was obtained as with the construct AB (Supplementary Fig. 3). Again, mature leaves were free of GUS activity (Supplementary Fig. 3C) and trichomes of young developing leaves exhibited an intense GUS staining (Supplementary Fig. 3D, E, G and H). In contrast to promoter construct AB, promoter construct C also reveals high GUS expression in young and older roots (Supplementary Fig. 3B and I), in particular at the root tips and in root hairs (Supplementary Fig. 3J). Moreover, GUS expression was also found in the vasculature of cotyledons (Supplementary Fig. 3C and G), which contrasts the lack of *ENO1* expression in cotyledons observed in RT-PCR experiments (Fig. 3A). Furthermore, with promoter construct C, there was also some GUS staining in the style (Supplementary Fig. 3K) and in the embryo sac (Supplementary Fig. 3L). As predicted from RT-PCR data, flowers lack *ENO1* expression completely (Fig. 3A), whereas developing siliques showed a transient increase in *ENO1* expression. The expression profile of *ENO1* is consistent with the idea that photosynthetic active chloroplasts lack a complete glycolysis to PEP, whereas certain plastids of non-green tissues, in particular those of developing seeds or in roots, are capable of generating PEP *via* glycolysis.

3.4. Homozygous eno1 knock-out mutants exhibit a distorted trichome morphology and reduced number of root hairs

In order to test the consequence of a deficiency in ENO1, two *eno1* mutant alleles were isolated from the SALK T-DNA insertion mutant collection and established as homozygous lines, *eno1-1* and *eno1-2* (Fig. 4A). Both mutant alleles lacked *ENO1* expression completely (Fig. 4B) and total ENO activity was reduced by 50% in roots, but not in leaves of *eno1-1* compared to the wild type (data not shown). On a macroscopic scale there were no differences in the phenotypes between the wild type and *eno1-1* or *eno1-2* (Supplementary Fig. 4A–C). Both shoot and root growth was unaffected when plants were grown on MS agar (Fig. 4E–H). However, a closer inspection of trichomes of young leaves revealed differences between mutant and wild-type plants. Trichomes of the mutants appeared less turgescent and had a distorted phenotype (Fig. 4D) as compared to the wild type (Fig. 4C). In particular, the occurence of a trichome phenotype in both *eno1-1* and *eno1-2* underlines the

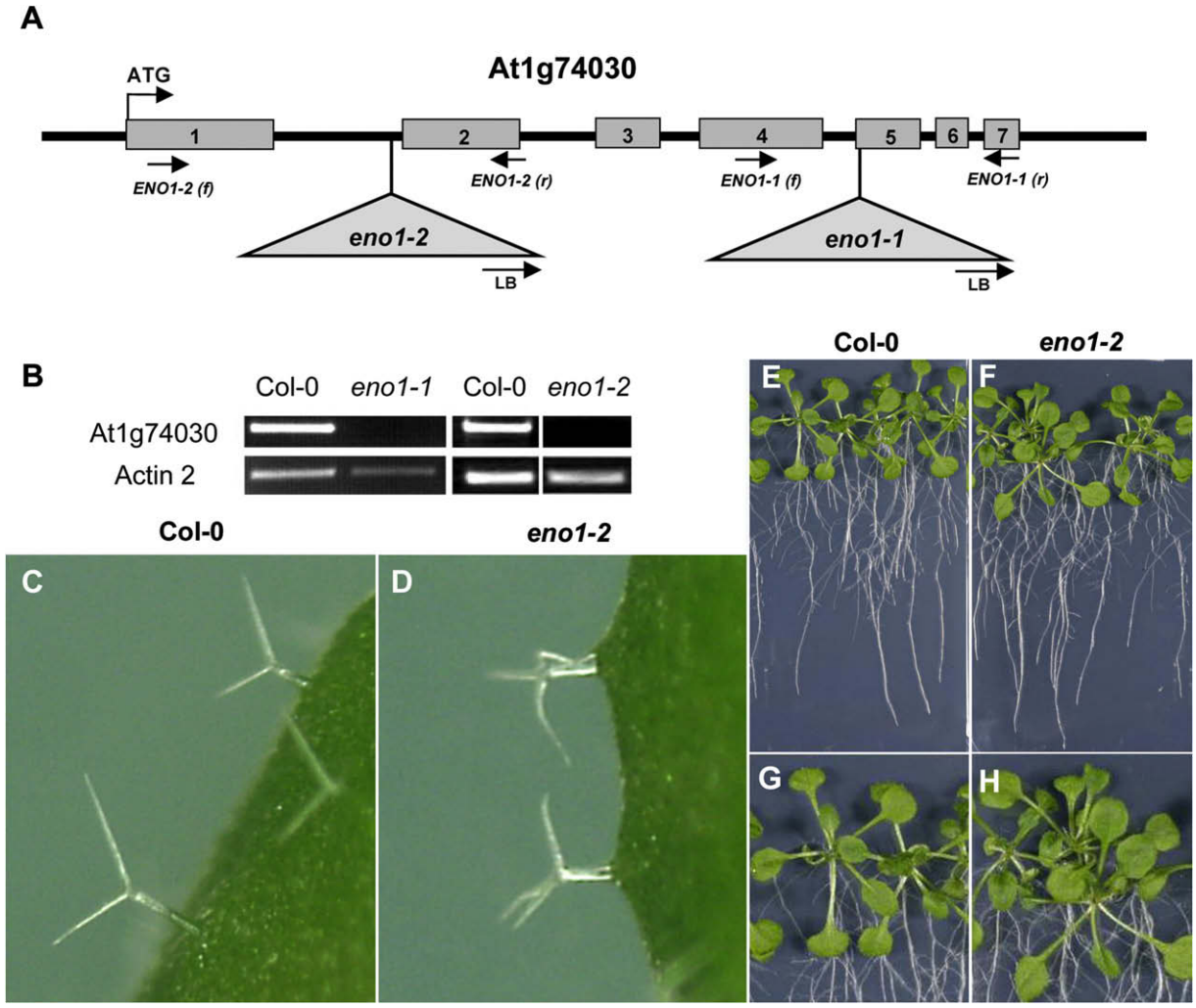

Fig. 4. Analyzes of T-DNA insertion mutants of *ENO1*. Two mutant alleles of *ENO1* (*eno1-1* and *eno1-2*) were isolated (A) and established as homozygous lines. The primer used for mutant screening are indicated by arrows (LB, T-DNA left border primer; ENO1-1(2) (f), forward = sense primer; ENO1-1(2) (r), reverse = antisense primer). Both lines lack *ENO1*-specific transcripts following RT-PCR (B). On a macroscopic scale the *eno1* plants lacked any phenotype different from the wild type (E–H). A closer inspection of young leaves revealed an aberrant, distorted shape of trichomes in *eno1* plants (D) compared to the wild type (C).

expression pattern observed in *ENO1* promoter::GUS plants (compare Fig. 3E and F). Furthermore, there was no significant difference in the root hair lengths between the mutant and the wild type (Supplementary Fig. 4D and E), but the number of root hairs was reduced by 17% in 2-week-old plants (data not shown) compared to the wild type, which might form a link to the expression of *ENO1* in non-root-hair cells as has been observed with the *ENO1 promotor::GUS* construct AB (compare Fig. 3H).

4. Discussion

We have identified and characterized the plastid-localized ENO from *A. thaliana* (AtENO1; At1g74030). The predicted plastid localization could be verified by transient expression of an ENO1-GFP fusion protein, which was found exclusively in plastids of cultured *A. thaliana* cells (Fig. 1A and B). In contrast, one of the two putative cytosolic enolases (ENOc; At2g36530) was found both in the cytosol and the nucleus (Supplementary Fig. 1A–D), which resembles the subcellular localization of the second putative cytosolic ENO (At2g36530), AtLOS2 [45]. It has been proposed that besides involvement of AtLOS2 in metabolism, it may also act as a transcriptional regulator. The respective homozygous *los2* mutant was severely impaired in growth, showed a pale green phenotype and was unable to develop flowers and subsequently siliques and seeds [45], underlining the importance of glycolytic PEP provision in the cytosol of plants. Here, the catalytic function of ENO1 could be verified with an enriched ENO1 preparation following heterologous expression of the ENO1 protein fused to a C-terminal His-tag in *E. coli*. The specific activity of ENO1 in the direction of PEP formation of 0.5–0.6 U mg^{-1} protein was relatively poor compared to reported values of up to 1000 U mg^{-1} protein for purified ENO from different organisms (http://www.brenda-enzymes.info/). However, control experiments with non-induced or wild-type *E. coli* cells revealed that ENO activity extracted from induced *E. coli* cells following purification by Ni–NTA chromatography was specifically due to the plant enzyme. The pH profiles of ENO1 activity, with an optimum between pH 7.0 and pH 8.0, and the apparent K_m values for both substrates, which were in the upper micromolar range, are consistent with ENO1 being functional in plastids *in vivo*.

The tissue-specific expression profile of *ENO1* supports the view that plastids from heterotrophic tissues, such as roots or developing seeds [31–34], contain a complete set of glycolytic enzymes, catalyzing for instance the breakdown of glucose 6-phosphate (Glc6P) to PEP (Fig. 5A and B; [48]), whereas in chloroplasts the conversion of 3-PGA to PEP is blocked due to the absence of ENO1 (Fig. 5C). Moreover, the analysis of wild-type *A. thaliana* plants expressing different *ENO1 promoter::reporter* gene constructs revealed a number of additional features on a cellular level, such as expression in trichomes of young leaves (construct AB and C) or in non-root-hair cells of the rhizodermis (construct AB). In particular construct AB, the fusion of the small intergenic 5′-fragment with the 3′-fragment, yielded the highest degree of overlaps between the GUS staining, RT-PCR experiments and expression profiles obtained from microarray data (i.e. http://bar.utoronto.ca/efp/cgi-bin/efpWeb.cgi). Enhancing effects of downstream sequences of cell-specific expression has already been reported for the *GLABROUS1* gene, a *MYB* gene homolog required for trichome initiation [41]. However, for the transcriptional regulation of *ENO1*, it remains to be shown whether all regulatory *cis*-acting elements are contained in construct AB. Further analyzes of *cis*-acting elements with the aid of 'PLACE Web Signal Scań (http://dna.affrc.go.jp/PLACE/signalscan.html; [49,50]) revealed a high number of known regulatory elements all over the gene.

Knock-out mutants of *ENO1* (*eno1-1* and *eno1-2*) lack a pronounced phenotype at the macroscopic scale, suggesting that ENO1 is redundant for plant development and metabolism, even in those tissues where *ENO1* transcripts are highly abundant, such as roots and siliques. Apart from glycolysis, PEP can be supplied from the cytosol *via* both AtPPTs, which are differentially expressed both in green and non-green tissues [20]. *AtPPT2*, for instance, is expressed throughout the leaf blade, but is absent in the roots, whereas *AtPPT1* shows high expression in the vasculature of roots and leaves as well as in the root tip and lateral root formation zones [20]. Moreover, both *AtPPT* genes are expressed at distinct stages during seed development (http://bar.utoronto.ca/efp/cgi-bin/efpWeb.cgi). Both At*ENO1* and *AtPPT1* are co-expressed during the early stage of embryo development, suggesting that PEP supply is shared by glycolytic conversion (e.g. from imported Glc6P, [51]) and by import from the cytosol via a PPT (see Fig. 5A). A similar shared function of PEP import and synthesis within the plastids is also conceivable for other non-green tissues. Hence, a double knock-out of both functions (i.e. ENO1 and the PPT) might have detrimental effects on the physiology and development of heterotrophic cells and tissues and probably on the whole plant. This issue is currently being addressed. For instance, in certain root cells the number of root hairs in the *eno1* mutant plants is reduced by 17% compared to

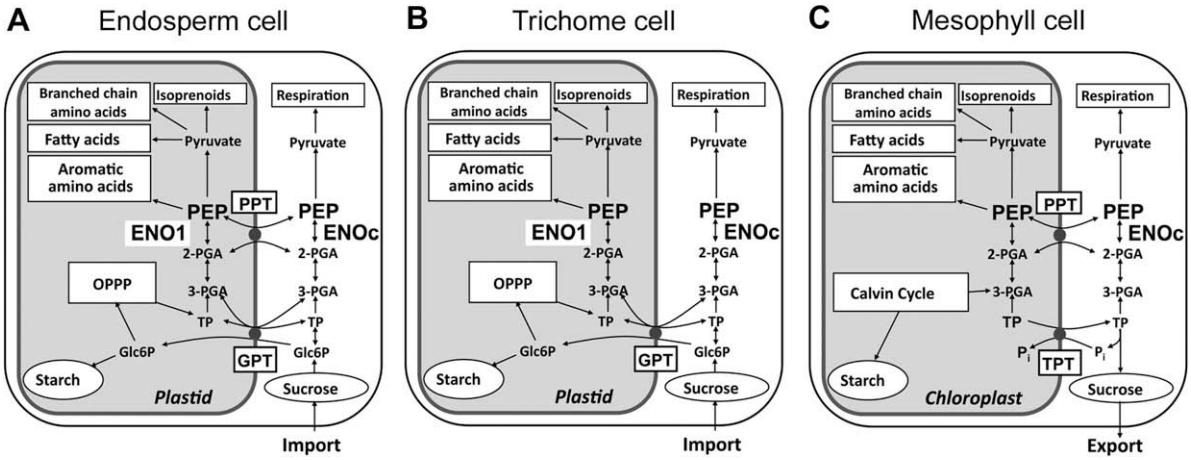

Fig. 5. Proposed paths of PEP supply to plastids and its fate in metabolism in different tissues of *A. thaliana*. In plastids of seed endosperm cells, PEP can either be imported from the cytosol via a PPT or generated by the glycolytic conversion starting from imported Glc6P (A). Trichome cells have to rely entirely on PEP provision by glycolysis (B), whereas chloroplasts from green tissues depend on the provision of PEP by the PPT (C). For the sake of clarity additional ways to generate PEP inside plastids (i.e. by PPDK) have been omitted.

the wild type indicating that a complete plastid glycolysis determines, at least partially, root hair formation. The expression profile of *ENO1* in trichomes as well as in non-root-hair cells (Fig. 3E and H) is similar to those of transcriptional regulators involved in trichome and root hair cell patterning [52,53]. There is, however, no obvious link between plastid glycolysis and developmental programs involved in cell patterning. Moreover, the distorted trichome phenotype observed in both alleles of the *eno1* mutants resembles in many aspects a group of mutants exhibiting aberrant trichome shapes based mainly on defective cytoskeleton formation [54–56]. It remains to be shown whether the distorted trichome phenotype in both *eno1* alleles is also caused by aberrant cytoskeleton development. Again, a direct link between a defective plastid glycolysis and cytoskeleton formation is missing. It is conceivable that in trichomes the glycolytic conversion of imported Glc6P [51] might be the only way to generate PEP in the plastid stroma, which then can be used as a precursor for the shikimate pathway or, after conversion to pyruvate *via* PK, for fatty acid biosynthesis, the synthesis of branched-chain amino acids or the synthesis of isoprenoids via the MEP pathway (Fig. 5B). The importance of ENO1 for PEP formation in plastids is supported by trichome specific microarray data. At the transcriptional level neither *AtPPT1* or *AtPPT2* nor *PPDK* could be detected, but *ENO1* was strongly up-regulated 3.8-fold compared to the residual epidermis cells [57], again supporting the *ENO1 promoter::GUS* studies. In contrast to heterotrophic plastids, chloroplasts produce 3-PGA during CO_2 fixation by ribulose-1,5-bisphosphate carboxylase/oxygenase. A simultaneous conversion of 3-PGA to PEP *via* PGyM and ENO1 rather than the reduction to triose phosphates during ongoing photosynthesis might hence be counterproductive for the export of photoassimilates from the chloroplasts or for the formation of transitory starch within the stroma (Fig. 5C). It is tempting to speculate that a fine tuning of leaf primary and secondary metabolism (i.e. PEP provision for the shikimate pathway) could be achieved at the level of chloroplast 3-PGA, 2-PGA and Pi concentrations in combination with cytosolic ENO activity. The stromal level of 3-PGA could hence determine the availability of 2-PGA via PGyM as a counter exchange substrate for the PPT, which in turn imports PEP generated from 2-PGA by cytosolic ENO (Fig. 5C). Therefore, chloroplast 3-PGA levels might indirectly determine the production of aromatic amino acids. This assumption will be tested by subcellular metabolite determinations in mutant or transgenic plants, which, for instance, express ENO1 in chloroplasts.

Acknowledgment

This work was supported by the Deutsche Forschungsgemeinschaft.

Appendix A. Supplementary data

Supplementary data associated with this article can be found, in the online version, at doi:10.1016/j.febslet.2009.02.017.

References

[1] Canback, B., Andersson, S.G.E. and Kurland, C.G. (2002) The global phylogeny of glycolytic enzymes. Proc. Natl. Acad. Sci. USA 99, 6097–6102.
[2] Plaxton, W.C. (1996) The organization and regulation of plant glycolysis. Annu. Rev. Plant Physiol. Plant. Mol. Biol. 47, 185–214.
[3] Givan, C.V. (1999) Evolving concepts in plant glycolysis: two centuries of progress. Biol. Rev. 74, 277–309.
[4] Edwards, G.E. and Nakamoto, H. (1985) Pyruvate, Pi dikinase and NADP–malate dehydrogenase in C4 photosynthesis: properties and mechanism of light/dark regulation. Annu. Rev. Plant Physiol. 36, 55–86.
[5] Chastain, C.J., Fries, J.P., Vogel, J.A., Randklev, C.L., Vossen, A.P., Dittmer, S.K., Watkins, E.E., Fiedler, L.J., Wacker, S.A., Meinhover, K.C., Sarath, G. and Chollet, R. (2002) Pyruvate, orthophosphate dikinase in leaves and chloroplasts of C_3 plants undergoes light-/dark-induced reversible phosphorylation. Plant Physiol. 128, 1368–1378.
[6] Hibberd, J.M. and Quick, W.P. (2002) Characteristics of C4 photosynthesis in stems and petioles of C3 flowering plants. Nature 415, 451–454.
[7] Parsley, K. and Hibberd, J.M. (2006) The *Arabidopsis* PPDK gene is transcribed from two promoters to produce differentially expressed transcripts responsible for cytosolic and plastidic proteins. Plant Mol. Biol. 62, 339–349.
[8] Sung, S.-J.S., Dian-Peng Xu, D.-P., Galloway, C.M. and Black, C.C. (1988) A reassessment of glycolysis and gluconeogenesis in higher plants. Physiol. Plant. 7, 650–654.
[9] Walker, R.P. and Chen, Z.-H. (2002) Phosphoenolpyruvate carboxykinase: structure, function and regulation. Adv. Bot. Res. 38, 93–189.
[10] Leegood, R.C. and Walker, R.P. (2003) Regulation and roles of phosphoenolpyruvate carboxykinase in plants. Arch. Biochem. Biophys. 414, 204–210.
[11] Fernie, A.S., Carrari, F. and Sweetlove, L.J. (2004) Respiratory metabolism: glycolysis, the TCA cycle and mitochondrial electron transport. Curr. Opin. Plant Biol. 7, 254–261.
[12] Herrmann, K.M. (1995) The shikimate pathway: early steps in the biosynthesis of aromatic compounds. Plant Cell 7, 907–919.
[13] Schmid, J. and Amrhein, N. (1995) Molecular organization of the shikimate pathway in higher plants. Phytochemistry 39, 737–749.
[14] Herrmann, K.M. and Weaver, L.M. (1999) The shikimate pathway. Annu. Rev. Plant Physiol. Plant Mol. Biol. 50, 473–503.
[15] Dennis, D.T. (1989) Fatty acid biosynthesis in plastids in: Physiology, biochemistry, genetics of non-green plastids (Boyer, C.D., Shannon, J.C. and Hardison, R.C., Eds.), pp. 120–129, American Society of Plant Physiologists, Rockville, MD.
[16] Ohlrogge, J.B. and Jaworski, J.G. (1997) Regulation of fatty acid synthesis. Annu. Rev. Plant Physiol. Plant Mol. Biol. 48, 109–136.
[17] Schulze-Siebert, D., Heineke, D., Scharf, H. and Schultz, G. (1984) Pyruvate-derived amino-acids in spinach-chloroplasts - synthesis and regulation during photosynthetic carbon metabolism. Plant Physiol. 76, 465–471.
[18] Lichtenthaler, H.K. (1999) The 1-deoxy-D-xylulose-5-phosphate pathway of isoprenoid biosynthesis in plants. Annu. Rev. Plant Physiol. Plant Mol. Biol. 50, 47–65.
[19] Fischer, K., Kammerer, B., Gutensohn, M., Arbinger, B., Weber, A., Häusler, R.E. and Flügge, U.-I. (1997) A new class of plastidic phosphate translocators: a putative link between primary and secondary metabolism by the phosphoenolpyruvate/phosphate antiporter. Plant Cell 9, 453–462.
[20] Knappe, S., Löttgert, T., Schneider, A., Voll, L., Flügge, U.-I. and Fischer, K. (2003) Characterization of two functional phosphoenolpyruvate/phosphate translocator (PPT) genes in *Arabidopsis* – AtPPT1 may be involved in the provision of signals for correct mesophyll development. Plant J. 36, 411–420.
[21] Streatfield, S.J., Weber, A., Kinsman, E.A., Häusler, R.E., Li, J., Post-Beittenmiller, D., Kaiser, W.M., Pyke, K.A., Flügge, U.-I. and Chory, J. (1999) The phosphoenolpyruvate/phosphate translocator is required for phenolic metabolism, palisade cell development, and plastid-dependent nuclear gene expression. Plant Cell 11, 1609–1622.
[22] Voll, L., Häusler, R.E., Hecker, R., Weber, A., Weissenböck, G., Fiene, G., Waffenschmidt, S. and Flügge, U.-I. (2003) The phenotype of the *Arabidopsis* cue1 mutant is not simply caused by a general restriction of the shikimate pathway. Plant J. 36, 301–317.
[23] Li, H., Culligan, K., Dixon, R.A. and Chory, J. (1995) CUE1: a mesophyll cell-specific positive regulator of light-controlled gene expression in *Arabidopsis*. Plant Cell 7, 1599–1610.
[24] Proudlove, M.O. and Thurman, D.A. (1981) The uptake of 2-oxoglutarate and pyruvate by isolated pea chloroplasts. New Phytol. 88, 255–264.
[25] Ohnishi, J.I., Flügge, U.-I., Heldt, H.W. and Kanai, R. (1990) Involvement of Na^+ in active uptake of pyruvate in mesophyll chloroplasts of some C_4 plants: Na^+/pyruvate cotransport. Plant Physiol. 94, 950–959.
[26] Stitt, M. and Ap Rees, T. (1979) Capacities of pea chloroplasts to catalyze the oxidative pentose–phosphate pathway and glycolysis. Phytochemistry 18, 1905–1911.
[27] Journet, E.P. and Douce, R. (1985) Enzymic capacities of purified cauliflower bud plastids for lipid-synthesis and carbohydrate-metabolism. Plant Physiol. 79, 458–467.
[28] Bagge, P. and Larsson, C. (1986) Biosynthesis of aromatic-amino-acids by aighly purified spinach-chloroplasts – compartmentation and regulation of the reactions. Physiol. Plant. 68, 641–647.
[29] Van der Straeten, D., Rodriguespousada, R.A., Goodman, H.M. and Van Montagu, M. (1991) Plant enolase – gene structure, expression, and evolution. Plant Cell 3, 719–735.
[30] Borchert, S., Harborth, J., Schünemann, D., Hoferichter, P. and Heldt, H.W. (1993) Studies of the enzymatic capacities and transport-properties of pea root plastids. Plant Physiol. 101, 303–312.
[31] Miernyk, J.A. and Dennis, D.T. (1982) Isozymes of the glycolytic-enzymes in endosperm from developing castor-oil seeds. Plant Physiol. 69, 825–828.
[32] Miernyk, J.A. and Dennis, D.T. (1992) A developmental analysis of the enolase isozymes from Ricinus communis. Plant Physiol. 99, 748–750.

[33] Kang, F. and Rawsthorne, S. (1994) Starch and fatty acid biosynthesis in plastids from developing embryos of oil seed rape. Plant J. 6, 795–805.
[34] Kang, F. and Rawsthorne, S. (1996) Metabolism of glucose-6-phosphate and utilization of multiple metabolites for fatty acid synthesis by plastids from developing oilseed rape embryos. Planta 199, 321–327.
[35] Mathur, J., Szabados, L., Schaefer, S., Grunenberg, B., Lossow, A., Jonas-Straube, E., Schell, J., Koncz, C. and Koncz-Kalman, Z. (1998) Gene identification with sequenced T-DNA tags generated by transformation of Arabidopsis cell suspension. Plant J. 13, 707–716.
[36] Koroleva, O.A., Tomlinson, M.L., Leader, D., Shaw, P. and Doonan, J.H. (2005) High-throughput protein localization in Arabidopsis using Agrobacterium-mediated transient expression of GFP-ORF fusions. Plant J. 41, 162–174.
[37] Laemmli, U.K. (1970) Cleavage of structural proteins during assembly of head of bacteriophage-T4. Nature 227, 680–685.
[38] Towbin, H., Staehelin, T. and Gordon, J. (1979) Electrophoretic transfer of proteins from polyacrylamide gels to nitrocellulose sheets: procedure and some applications. Proc. Natl. Acad. Sci. USA 76, 4350–4354.
[39] Bradford, M.M. (1976) Rapid and sensitive method for quantitation of microgram quantities of protein utilizing principle of protein-dye binding. Anal. Biochem. 72, 248–254.
[40] Ausubel, F.M., Brent, R., Kingston, R.E., Moore, D.D., Seidman, J.G., Smith, J.A. and Struhl, K. (1990) Current Protocols in Molecular Biology, Wiley, New York.
[41] Larkin, J.C., Oppenheimer, D.G., Pollock, S. and Marks, M.D. (1993) *Arabidopsis* GLABROUS1 gene requires downstream sequences for function. Plant Cell 5, 1739–1748.
[42] Bailey-Serres, J. and Dawe, R.K. (1996) Both 5′ and 3′ sequences of maize adh7 mRNA are required for enhanced translation under low-oxygen conditions. Plant Physiol. 112, 685–695.
[43] Jefferson, R.A., Kavanagh, T.A. and Bevan, M.W. (1987) GUS fusions: ß-glucuronidase as a sensitive and versatile gene fusion marker in higher plants. EMBO J 6, 3901–3907.
[44] Schwacke, R., Schneider, A., van der Graaff, E., Fischer, K., Catoni, E., Desimone, M., Frommer, W.B., Flügge, U.-I. and Kunze, R. (2003) ARAMEMNON: a novel database for *Arabidopsis thaliana* integral membrane proteins. Plant Physiol. 131, 16–26.
[45] Lee, H., Guo, Y., Ohta, M., Xiong, L., Stevenson, B. and Zhu, J.K. (2002) LOS2, a genetic locus required for cold-responsive gene transcription encodes a bi-functional enolase. EMBO J. 21, 2692–2702.
[46] Segel, I.H. (1993) Enzyme Kinetics. Behavior and Analysis of Rapid Equilibrium and Steady-state Enzyme Systems, John Wiley and sons Inc., New York.
[47] Bergmeyer, H.U. (1970) in: Methoden der enzymatischen Analyse (Bergmeyer, H.U., Ed.), Verlag Chemie, Weinheim.
[48] Ruuska, S.A., Girke, T., Benning, C. and Ohlrogge, J.B. (2002) Contrapuntal networks of gene expression during *Arabidopsis* seed filling. Plant Cell 14, 1191–1206.
[49] Prestridge, D.S. (1991) SIGNAL SCAN: a computer program that scans DNA sequences for eukaryotic transcriptional elements. CABIOS 7, 203–206.
[50] Higo, K., Ugawa, Y., Iwamoto, M. and Korenaga, T. (1999) Plant cis-acting regulatory DNA elements (PLACE) database:1999. Nuclear Acids Res. 27, 297–300.
[51] Kammerer, B., Fischer, K., Hilpert, B., Schubert, S., Gutensohn, M., Weber, A. and Flügge, U.-I. (1998) Molecular characterization of a carbon transporter in plastids from heterotrophic tissues: the glucose 6-phosphate/phosphate antiporter. Plant Cell 10, 105–117.
[52] Schellmann, S., Schnittger, A., Kirik, V., Wada, T., Okada, K., Beermann, A., Thumfahrt, J., Jürgens, G. and Hülskamp, M. (2002) TRIPTYCHON and CAPRICE mediate lateral inhibition during trichome and root hair patterning in *Arabidopsis*. EMBO J. 21, 5036–5046.
[53] Kirik, V., Simon, M., Hülskamp, M. and Schiefelbein, J. (2004) The ENHANCER OF TRY AND CPC1 gene acts redundantly with TRIPTYCHON and CAPRICE in trichome and root hair cell patterning in *Arabidopsis*. Dev. Biol. 268, 506–513.
[54] Hülskamp, M., Misera, S. and Jürgens, G. (1994) Genetic dissection of trichome cell development in *Arabidopsis*. Cell 76, 555–566.
[55] Mathur, J., Spielhofer, P., Kost, B. and Chua, N.H. (1999) The actin cytoskeleton is required to elaborate and maintain spatial patterning during trichome cell morphogenesis in *Arabidopsis thaliana*. Development 126, 5559–5568.
[56] Schwab, B., Mathur, J., Saedler, R., Schwarz, H., Frey, B., Scheidegger, C. and Hülskamp, M. (2003) Regulation of cell expansion by the DISTORTED genes in *Arabidopsis thaliana*: actin controls the spatial organization of microtubules. Mol. Gen. Genom. 269, 350–360.
[57] Jakoby, M.J., Falkenhan, D., Mader, M.T., Brininstool, G., Wischnitzki, E., Platz, N., Hudson, A., Hülskamp, M., Larkin, J. and Schnittger, A. (2008) Transcriptional profiling of mature *Arabidopsis* trichomes reveals that NOECK encodes the MIXTA-like transcriptional regulator MYB106. Plant Physiol. 148, 1583–1602.